JACS
JOURNAL OF THE AMERICAN CHEMICAL SOCIETY
Article
pubs.acs.org/JACS

Dual-Mode Ultrasensitive Quantification of MicroRNA in Living Cells by Chiroplasmonic Nanopyramids Self-Assembled from Gold and Upconversion Nanoparticles

Si Li,[†,#] Liguang Xu,[†,#] Wei Ma,[†] Xiaoling Wu,[†] Maozhong Sun,[†] Hua Kuang,[*,†] Libing Wang,[†] Nicholas A. Kotov,[‡] and Chuanlai Xu[†]

[†]State Key Lab of Food Science and Technology, International Joint Research Laboratory for Biointerface and Biodetection, School of Food Science and Technology, Jiangnan University, Wuxi, Jiangsu 214122, People's Republic of China

[‡]Department of Chemical Engineering, University of Michigan, Ann Arbor, Michigan 48109-2136, United States

Supporting Information

ABSTRACT: Chiral self-assembled nanomaterials with biological applications have attracted great interest. In this study, DNA-driven gold-upconversion nanoparticle (Au-UCNP) pyramids were fabricated to detect intracellular microRNA (miRNA) in real time. The Au-UCNP pyramids are doubly optically active, displaying strong plasmonic circular dichroism (CD) at 521 nm and significant luminescence in 500−600 nm, and therefore can be monitored by both of them. CD will decrease while the luminescence intensity increases in the presence of miRNA. The experimental results show that the CD intensity had an outstanding linear range from 0.073 to 43.65 fmol/10 μg_{RNA} and a limit of detection (LOD) of 0.03 fmol/10 μg_{RNA}, whereas the luminescence intensity ranged from 0.16 to 43.65 fmol/10 μg_{RNA} with a LOD of 0.12 fmol/10 μg_{RNA}. These data indicate that the CD signal is much more sensitive to the concentration of miRNA than the luminescent signal, which is attributed to the strong CD intensity arising from the spin angular momentum of the photon interaction with chiral nanostructures and the plasmonic enhancement of the intrinsic chirality of DNA molecules in the pyramids. This approach opens up a new avenue to the ultrasensitive detection and quantification of miRNA in living cells.

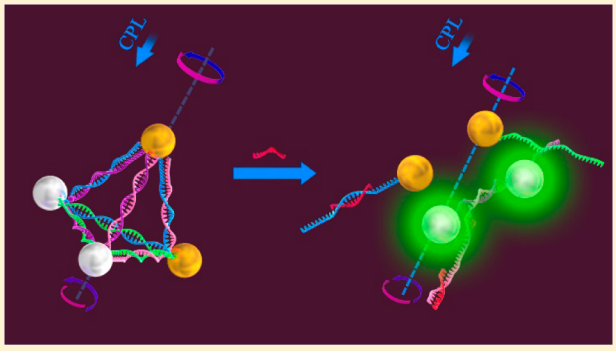

INTRODUCTION

MiRNAs are endogenous, short, noncoding, regulatory RNAs that play important roles in numerous biological processes.[1,2] It is universally acknowledged that changes in miRNA expression levels are associated with various pathological conditions.[3−5] In particular, miRNAs are diversely expressed in many solid tumors, and the expression levels of one or more miRNAs are commonly used as important diagnostic and prognostic biomarkers.[6,7] However, their intrinsic characteristics, including low abundance, ready degradation, small sizes, and similarity in sequences among family members, make developing an ultrasensitive, highly selective, and *in situ* method to quantify the intracellular levels of microRNAs extremely challenging, despite its urgent need.

Quantitative real time (RT) polymerase chain reaction (PCR) and microarray hybridization are two methods commonly used to measure aberrant miRNA expression.[8] In spite of their significant advantages with sensitivity and high throughput, they are limited by their high cost, complex operative processes, and requirement for skilled operators. Simpler quantification approaches have been developed, such as DNA-gold nanoparticle probes, the two-stage isotachophoresis assay, and so on,[9−13] but these methods require miRNA to be extracted from cells prior to analysis or measurement outside the cell. Recently, a few of RNA detection probes, labeled with fluorescent dyes for *in situ* visualization and localization, have been developed, such as the hybridization chain reaction (HCR),[14] nanosnail-inspired nucleic acid locator,[15] duplex-specific nuclease signal amplification,[16] fluorescence resonance energy transfer (FRET) nanoflares,[17] and gold@polydopamine core−shell nanoprobes.[18] However, they have focused on the imaging and qualitative detection of RNA in living cells.[19−21] Although Haifeng Dong and co-workers reported an *in situ* quantification method using a multifunctional SnO_2 probe with carboxyfluorescein (FAM) fluorescence as the detection signal, background autofluorescence and the optical instability of fluorescent dyes are still serious limitations to the intracellular quantification of miRNA.[22,23]

Well-defined nanostructures in which the nanoparticles undergo controlled self-assembly have regular geometric shapes, structural stability, and strong optical activity.[24] Based on these promising properties, the self-assembled nanostructures have been used extensively as biosensors.[25−33] However

Received: October 15, 2015
Published: December 21, 2015

DOI: 10.1021/jacs.5b10309
J. Am. Chem. Soc. 2016, 138, 306−312

Scheme 1. (A) Working Principle of Au-UCNP Pyramids for miRNA Detection and (B) the Nucleic Acid Skeleton of Pyramid Used for miRNA Detection[a]

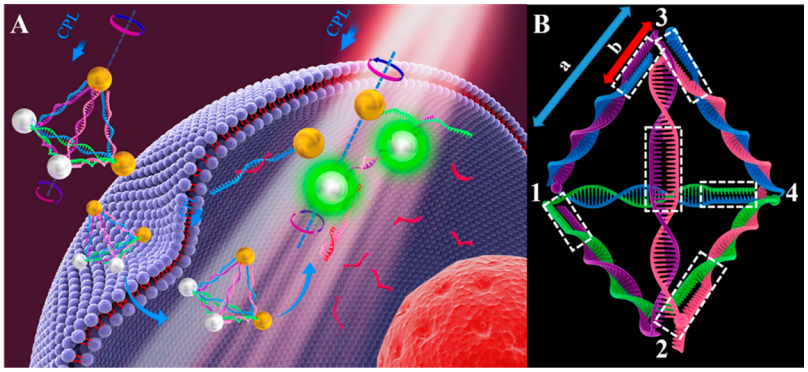

[a]3, 4 are linked with Au NPs; 1, 2 are linked with UCNPs. Part a: Recognition sequence of miRNA; and part b: non-complemented part (circled by white dashed line).

the detection of intracellular miRNAs based on nanoassemblies has not yet been reported. The plasmonic chiroptical properties of the nanostructures have been a topical issue in recent years that has drawn much attention.[34−41] Our group has constructed many chiral nanoscale assemblies and developed a series of ultrasensitive detection methods for nucleic acid fragments and cancer biomarkers *in vitro*.[42−44] However, their biological applications in living cells are yet to be explored.

In this study, we constructed DNA-driven self-assembled pyramids (denoted "Au-UCNP pyramids") between gold nanoparticles (Au NP, 20 ± 3 nm, aspect ratio, 1:1.2) and upconversion nanoparticles (UCNP: $NaGdF_4$:Yb^{3+}, Er^{3+}, 19 ± 3 nm). Lanthanide-doped UCNPs were chosen as one building block in the pyramids because of their unique optical properties, excitation with near-infrared light, anti-Stokes emission, superior photostability and chemical stability, low toxicity, and high signal-to-noise ratios, all of which are obvious advantages over fluorescent dyes.[45−57] With the prolate geometry of the Au NPs, the assembled pyramids display chiroptical activities, consistent with our previous research.[42,44] To be noticed, the chiroptical response of intracellular substances is only optically active in the ultraviolet (UV) region of the absorbance spectrum, with no overlapping interference from the chiroplasmonic properties of the pyramids in the visible region. The luminescence of UCNPs is quenched in the pyramids by the luminescence resonance energy transfer (LRET) between the Au NPs and UCNPs.[58,59] With the CD and luminescent signals of the Au-UCNP pyramids and the ingenious design of the DNA frame, we achieved ultrasensitive and highly selective detection of miRNA in live cells based on their dual mode signaling.

RESULTS AND DISCUSSION

Principle of the Dual-Signals of Intracellular miRNA Quantitation. The underlying principle of the quantitative detection of intracellular miRNAs with Au-UCNP pyramids is illustrated in Scheme 1. First, the miRNA recognition sequences are embedded in each side of the DNA frame (part a in Scheme 1B); part b in Scheme 1B is non-complementary (in each side of the DNA frame, it is circled by white dashed line). When miRNA is present, it will be complementary to the recognition sequence on each side, which leads to the complete dissociation of the DNA frame (the Au-UCNP pyramid is assembled with the sequences from 1 to 4, see the Supporting Information (SI)). The Au NPs and UCNPs in the pyramid are then separated from one another, the chiroplasmonic activities of pyramid disappears, and the luminescence of the UCNPs is restored (Scheme 1A).

Structural and Optical Characterization of Au-UCNP Pyramids. The pyramids were assembled as follows. First, two homogeneous Au NP and UCNP pairs were formed (Figure S1C,D). The two dimers were then hybridized to assemble the Au-UCNP pyramids (Figure 1A). Representative transmission electron microscopy (TEM) images show the successful preparation of the Au-UCNP pyramids (Figure S2A). A statistical analysis of up to 100 TEM images indicated that the yields for the Au-UCNP pyramid were as high as 85%. This was also confirmed by bathochromic shift of the gold absorbance band from 519 to 521 nm in the UV−vis spectrum (Figure S1F). The spatial configuration of the Au-UCNP pyramid was characterized by three-dimensional (3D) reconstruction with cryo-electron tomography (Figures 1B and S2B). The stability of the Au-UCNP pyramids was observed in cell culture medium (Figure S1E), in which thiolated polyethylene glycol (PEG-SH, molecular weight, 5000) and cell-penetrating peptide (TAT) were coated onto individual particles. Concurrently, the self-assembled pyramids showed a strong CD signal (Figure 1C). The luminescence of the UCNPs in the pyramids was significantly quenched because of the LRET between the Au NPs and UCNPs (Figure 1D). We noted that the mixture of Au NPs and UCNPs (molar ratio: 1:1), which was similar to the mixture of Au NPs and UCNPs that dissociated from the pyramids, had no CD signal but displayed strong luminescence intensity (Figure 1C,D).

Performance Evaluation of miRNA Detection *in Vitro*. MiR-21, recognized as an "oncomir" attributed to its over-expression levels, has been indicated to elaborate the sensitivity to different anticancer agents.[60] Therefore, miR-21 was used as the model miRNA in the following experiments. First, the target (microRNA-21) was used to verify the feasibility of the detection strategy *in vitro*, and the results showed that the dual CD and luminescent signals both demonstrated perfect linear relationships with the miR-21 concentration in the range of 2−50 pM (Figures 2A,B and S3A,B). And then, two mutated sequences of miR-21, let-7, and miR-200b (sequences 5−9, see SI) were used as the four control groups to test the selectivity of the Au-UCNP pyramids. In the presence of miR-21, the CD signal disappeared, and the luminescent signal was restored,

DOI: 10.1021/jacs.5b10309
J. Am. Chem. Soc. 2016, 138, 306−312

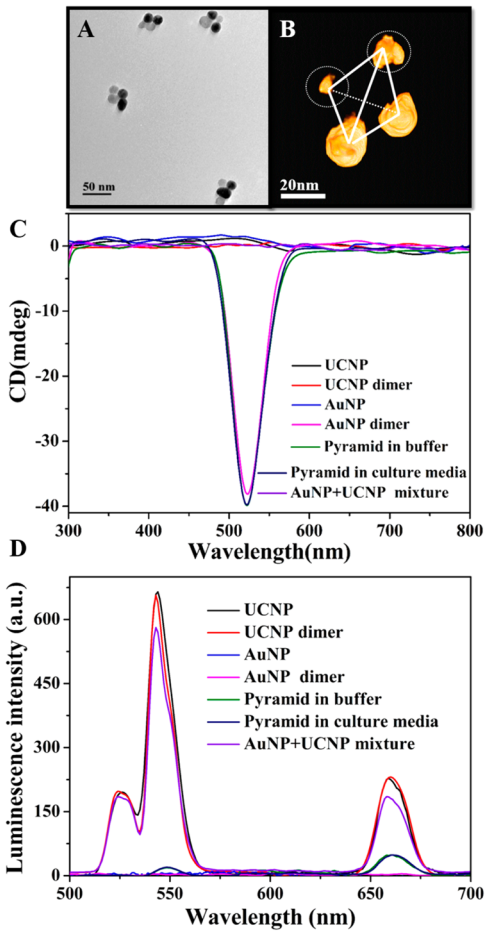

Figure 1. (A) TEM images of pyramids assembled with Au NPs and UCNPs in 10 mM Tris buffer. (B) 3D reconstruction cryo-TEM tomography image of pyramids. (C) CD and (D) luminescence spectra of Au NP, UCNP, Au NP-DNA, UCNP-DNA, Au NP dimers, UCNP dimers, Au NP + UCNP mixture, pyramids in 10 mM Tris buffer and in cell culture medium upon irradiation with 980 nm NIR laser (0.8W).

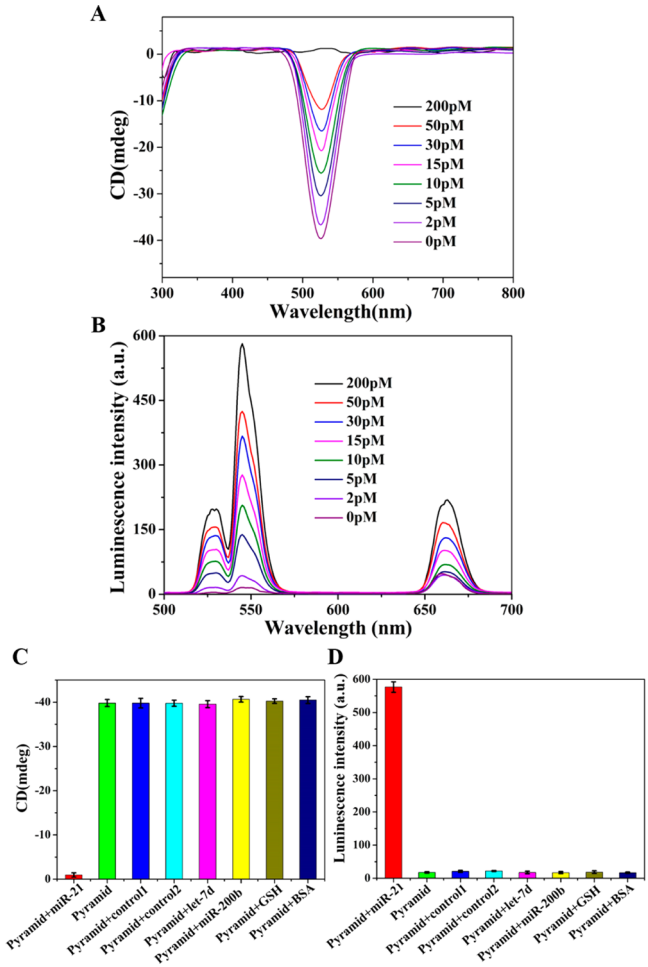

Figure 2. (A) CD and (B) luminescence spectra of Au-UCNP pyramids responded to different concentrations of miR-21 (0, 2, 5, 10, 15, 30, 50, or 200 pM) *in vitro*. (C) CD (521 nm) and (D) luminescence intensity (543 nm) of Au-UCNP pyramids responded to the excess miR-21 (200 pM), mutated sequences of miR-21 (200 pM, control 1, control 2), let-7d (200 pM), miR-200b (200 pM), BSA (2 mM), and GSH (2 mM) *in vitro*. The luminescence intensity of the samples was obtained upon irradiation with 980 nm NIR laser (0.8 W).

whereas no obvious changes in the CD or luminescent signals were observed in the control groups, suggesting that this detection probe had an excellent specificity (Figures 2C,D and S3C,D). Bovine serum albumin (BSA), a typical protein, and glutathione (GSH) were then used to spike the detection system, and no change in the CD or luminescent signals was observed. This implies that the pyramid nanostructures experienced almost no interference from proteins or peptides because they could not break the Au−S bonds between ssDNA and AuNPs and maleinimide−S bonds between ssDNA and UCNPs (Figures 2C,D and S3C,D).

Stability and Cytotoxicity of Au-UCNP Pyramids. Pyramids with modified phosphorothioate bonds in the DNA skeleton displayed significant stability, resisting enzymatic lysis (Figures S4 and S5). The marked stability of the pyramids may prevent nonspecific signals produced by intracellular nuclease activity. The pyramids also displayed negligible cytotoxicity and had almost no effect to the viability of living cells (Figure S6). These results lay a solid foundation for the real-time intracellular detection of miRNAs in living cells.

Cellular Uptake of Au-UCNP Pyramids. Human epithelial cancer cells (HeLa cells) were selected for the intracellular miR-21 analysis because they are quintessential carcinoma cells known to express high levels of miR-21.[60] To monitor the uptake efficiency and the dynamics of the pyramids in living cells, two kinds of pyramidal probes with different DNA frames were fabricated. The as-prepared probe (probe 1) was assembled with sequences that specifically hybridized to the target (sequences 1−4, see SI), and the other probe (probe 2) was designed with no ability to capture the target miR-21, as the control probe (sequences 10−13, see SI). To track the dynamics of the pyramids in living cells, the intracellular CD and luminescent signals for the two types of probes were recorded during different periods. In the presence of intracellular miR-21, the intracellular CD signal detected with probe 1 (CD1) was lower than that detected with probe 2 (CD2), the value of ΔCD (ΔCD = |CD2| − |CD1|) continued to increase for 8 h (Figure 3A−C), and the luminescence intensity (probe 1) was strongest at 8 h (Figure 4A). However, the control group (probe 2) had a less luminescent optical signal (Figure 4B). These results provide convincing evidence that probe 1 specifically recognized the target, but the probe 2 did not. Both signals then became stable until 20 h (Figures 3C and 4A), and

DOI: 10.1021/jacs.5b10309
J. Am. Chem. Soc. 2016, 138, 306−312

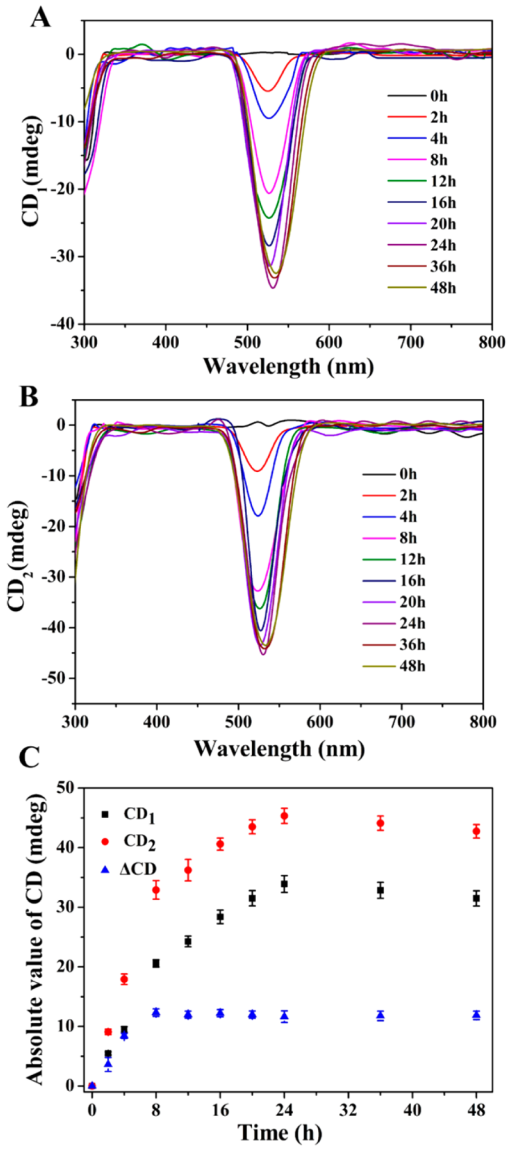

Figure 3. Intracellular CD spectra for different time incubated with probes (A) 1 and (B) 2. (C) Statistics of CD signal (521 nm). Probe 1: Assembled with the sequences that could specifically hybridize with miR-21 as described in Scheme 1B. Probe 2: Assembled with absolute complementary sequences that had no ability to recognize miR-21.

the UV−vis peak and the CD bands did not shift during this period (Figures 3A,B and S7A,B), suggesting that the pyramids have excellent dispersity in living cells. Bio-TEM images provided further evidence of this (Figure S7C,D). However, the UV−vis and CD bands for both probes became wide after 20 h, and displayed apparent 9 nm red shifts relative to those before 20 h from 521 to 530 nm (Figures 3A−C and S7A,B), and the luminescence intensity in the confocal images decreased after 20 h. This could be attributed to the aggregation of the pyramids in the cells (Figure S7C). All these results imply that 8 h is the optimal time for the detection of intracellular miR-21.

Live Cell miRNAs Sensor. To determine the various levels of miR-21 in living cells, HeLa cells were transfected with different amounts of miR-21 using a commercial transfection agent (lipofectamine RNAiMAX transfection reagent) to increase the miR-21 levels or with the antisense sequence corresponding to miR-21 to reduce the miR-21 levels. After

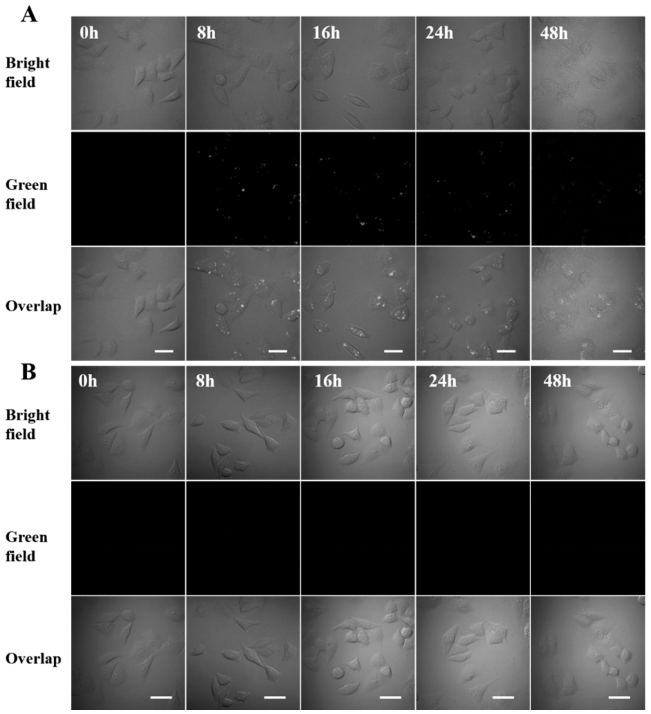

Figure 4. (A) Confocal images of probe 1 in HeLa cells with different incubated time. (B) Confocal images of Probe2 in HeLa cells with different incubated time. Scale bar =20 μm.

transfection, the amounts of intracellular miR-21 were quantified with quantitative RT-PCR (qRT-PCR) (Figure S9A−C). We noted that the original content of miR-21 in living HeLa cells was 3.181 fmol/10 μg_{RNA} (fmol/10 μg_{RNA} is equal to fmol/10^6 cells). The intracellular CD signal and confocal images were obtained after the HeLa cells expressing different levels of miR-21 were incubated with the Au-UCNP pyramids (Figure 5A,B). As evident in the CD spectra and confocal images, the CD intensity decreased as the concentration of miR-21 increased in the cells, whereas the florescence intensity increased. Both signals showed good linear relationships with the concentration of miR-21(Figure 5C,D). The detection range of the CD signal was calculated to be 0.073−43.64 fmol/10 μg_{RNA}, and the LOD was 0.03 fmol/10 μg_{RNA}, respectively. Importantly, when miR-21 reached 0.073 fmol/10 μg_{RNA}, the luminescence intensity of the confocal image was too weak to be detected. The luminescent signal only showed a linear relationship between 0.16 and 43.64 fmol/10 μg_{RNA}, and the LOD was 0.12 fmol/10 μg_{RNA}. The sensitivity of CD detection was four times higher than that of luminescent detection in live HeLa cells. The ultralow LOD of the CD method may be attributable to the following four factors: plasmon−plasmon coupling of the AuNPs of the pyramids, which is a dominant factor;[24,34−39] the induced plasmonic CD by exciton−plasmon coupling;[41−43] the hybrid dipole−dipole coupling between the UCNPs and AuNPs; and the minimal interference from the matrix.

Human breast cancer cells (MCF-7) and primary uterine fibroblast cells (PCS-460-010) were used to test the reliability of the developed method. From the CD spectra and confocal images obtained (Figure 6A,B), we quantified the levels of miR-21 in these two cell lines through the standard curves in Figure 5C,D. The plasmonic CD and luminescence detection results for the MCF-7 cells were 12.11 ± 0.11 and 11.23 ± 0.39 fmol/

DOI: 10.1021/jacs.5b10309
J. Am. Chem. Soc. 2016, 138, 306−312

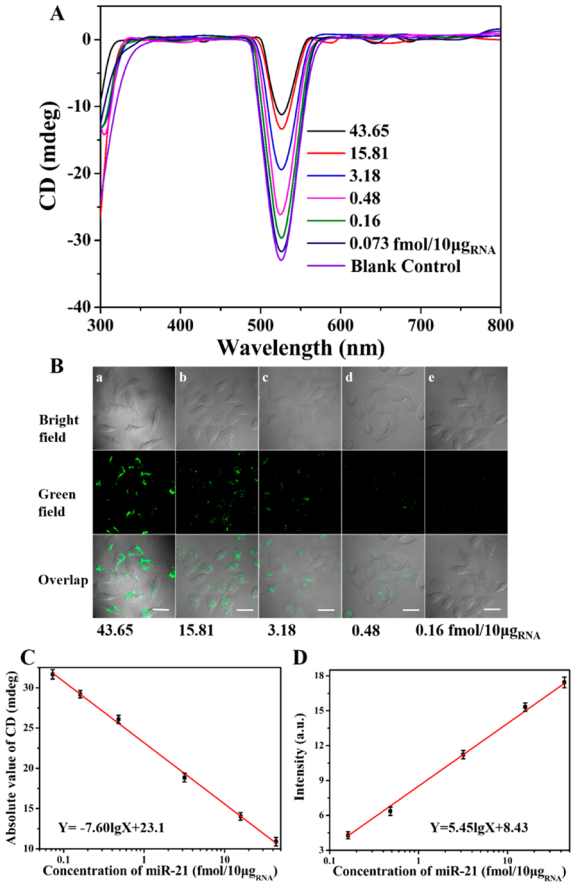

Figure 5. (A) CD spectra and (B) confocal images of HeLa cells with different amounts of miR-21 (a and b were transfected with miR-21; c was not transfected; d and e were transfected with antisense sequences of miR-21, respectively) with probe 1. Note that blank control in (A) was totally inhibited with excess antisense sequences of miR-21 which could not be detected by qRT-PCR. Plot of (C) CD (521 nm) and (D) luminescence intensity versus the different concentrations of intracellular miR-21, the continuous-wave near-infrared laser operating at 980 nm provided the excitation, and luminescence was collected at 540 ± 60 nm. Scale bar = 20 μm.

10 $\mu g_{RNA,}$ respectively (74.7 ± 0.7 and 67.6 ± 2.4 copies/ng_{RNA} × 10^4, respectively), which were approximately three times higher than those for HeLa cells. For the normal PCS-460-010 cells, these were calculated to be 0.056 ± 0.003 fmol/10 μg_{RNA} (33.7 ± 1.8 copies/ng_{RNA} × 10^2) with plasmonic CD, but could not be detected with the luminescent signal because the sensitivity of the luminescent signal was lower than that of the CD signal. These results are consistent with the reported values.[9,61] These findings are convincing evidence that this ultrasensitive and feasible chiral-nanostructure-based detection method can be applied to biological systems.

CONCLUSION

In conclusion, an ultrasensitive and selective method for the detection of miRNA has been developed based on chiroplasmonic and upconversion luminescence properties of Au-UCNP pyramids as intracellular nanoprobes. With dual plasmonic CD and luminescent signals, the nanoprobe not only visualizes and localizes the target but also detects abnormal endogenous miRNA *in situ* quantitation in live cells. It is noteworthy that plasmonic CD detection has a significantly much higher sensitivity than luminescence detection, suggesting that chiral nanoscale assemblies are potential probes for intracellular bioanalysis. We believe that these heterogeneous assembled nanostructures with chiroplasmonic properties hold great promise for the investigation of intracellular biomarkers, signaling molecules, and even the dynamic biological processes of living cells. And the strategy is expected to facilitate the developments of chiral nanomaterials in biological applications.

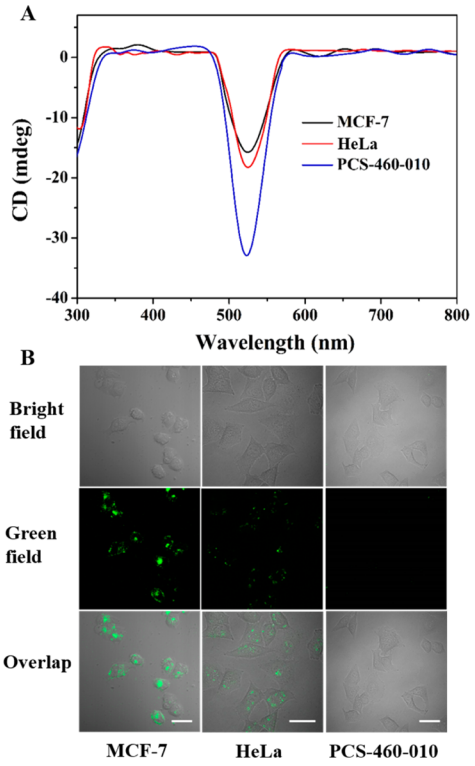

Figure 6. (A) CD spectra and (B) confocal images of MCF-7, HeLa, PCS-460-010 cells with Au-UCNP pyramids. Scale bar = 20 μm.

EXPERIMENTAL SECTION

Preparation of Au-UCNP Pyramids. Au NPs prepared were functionalized with thiolated single-stranded DNA (ssDNA) which modified with phosphorothioate bonds, according to a previously reported method.[43] The Au NPs were mixed with ssDNA in a ratio of 1:3.5 and incubated for 12 h in 0.5 × TBE (89 mM Tris-borate, 89 mM boric acid, 2 mM EDTA) and 50 mM NaCl. The samples were then centrifuged at 8000 *g* for 10 min to remove any uncoupled oligonucleotide from the solution. The supernatant was removed, and the pellet was resuspended in water.

The PEG-protected UCNPs were mixed with ssDNA in a ratio of 1:3.5 and incubated for 12 h in 10 mM Tris buffer and 50 mM $NaNO_3$. The samples were then centrifuged at 13,000 *g* for 20 min to remove any uncoupled oligonucleotide. The supernatant was removed, and the pellet was resuspended in water.

In the first stage, Au NP and UCNP dimers were prepared. Two identical Au NP-DNA conjugates bearing partially complementary ssDNA were mixed together in 10 mM Tris buffer, 50 mM $NaNO_3$, and 10 mM $Mg(NO_3)_2$ buffer, heated at 90 °C for 5 min, and then hybridized for 12 h at room temperature. The same procedure was used for the preparation of the UCNP dimers.

In the second stage, Au NP-UCNP pyramids were assembled by hybridizing the Au NP dimers and UCNP dimers and stirring the mixture for 24 h at room temperature to obtain the desired Au-UCNP pyramids. All the pyramids used in the whole study were fabricated with the process described above.

Functionalization of Au-UCNP Pyramids. Thiol-functionalized polyethylene glycol (PEG-SH, molecular weight: 5000) solution was

DOI: 10.1021/jacs.5b10309
J. Am. Chem. Soc. 2016, 138, 306−312

added to the pyramid solution in a PEG:pyramids molar ratio of 1000:1. After 15 min, excess PEG was removed with three rounds of centrifugation at 10,000 *g* for 10 min and washed with distilled water. Cell-penetrating peptide (TAT, 10 mM) was then added to the PEG-coated pyramid solution at a peptide: NPs molar ratio of 1000:1 and incubated for 24 h at room temperature. The excess peptide was removed, and the sample washed three times with distilled water and centrifuged at 13,000 *g* for 20 min.

Response of Pyramids to miRNA-21 (miR-21) *in Vitro*. MiRNA target (miR-21) with various concentrations, two types of control RNAs mimicking miR-21 sequences (named by controls 1 and 2, respectively), let-7d, miRNA-200b (miR-200b), bovine serum albumin (BSA), and glutathione (GSH) were added to detection solution for 1 h (or 24 h for the BSA and GSH samples) at 37 °C, respectively, and the luminescent and CD signals were measured after the reaction.

To determine the sensitivity of detection *in vitro*, the pyramids in 10 mM Tris buffer were spiked with different concentrations of miR-21 (0, 2, 5, 10, 15, 30, 50, or 200 pM). After incubation for 1 h at 37 °C, the luminescent and CD signals were monitored.

Evaluation the miR-21 Expressed Level in Cancer and Normal Cell Lines. HeLa (human epithelial carcinoma line), MCF-7 (human breast cancer line), and PCS-460-010 cells (human epithelial normal line) were purchased from the American Type Culture Collection (Manassas, VA). The cells were cultured in Dulbecco's modified Eagle's medium containing 10% fetal bovine serum and 1% penicillin/streptomycin at 37 °C under a 5% CO_2 atmosphere. The cell numbers were counted with a Petroff-Hausser cell counter (USA). Serum-free medium (Opti-MEM) was used during the transfection process.

Construction of Intracellular miRNA CD Assay. HeLa cells were seeded in six-well plates at a density of 10^5 cells/well and cultured for 12 h before use. Pyramids (25 nM) were cultured with the cells. After culture, the cells were collected with trypsinization and washed three times with cold PBS to remove the extracellular pyramids. The cells were then redispersed in cold PBS and adjusted to the equal cell concentration (10^6 cells per assay). The CD signals of the treated cells were characterized with a MOS-450/AF-CD spectrometer. The optical path length was 1 cm.

Intracelluar miRNA Imaging Using Confocal Fluorescence Microscopy. HeLa cells were seeded in Petri dishes at a density of 10^5 cells/dish and cultured for 12 h before use. The cells were then incubated with 25 nM pyramids. After culture, the cells were washed three times with cold PBS to remove the extracellular pyramids. Confocal images of the treated cells were obtained with a confocal fluorescence microscopy. To avoid unnecessary damage to the cells, the microscope shutter was opened only long enough to allow the laser to illuminate the bound cells while the luminescent image was collected. The luminescence of the pyramids was excited at 980 nm, and the luminescent signals were collected at 500−600 nm.

Transfection of miR-21 and Antisense Sequences of miR-21 into HeLa Cells. The transfection process was performed according to the instructions for RNAiMAX. Briefly, HeLa cells were incubated for 48 h with Opti-MEM containing RNAiMAX and miR-21 mimics or RNAiMAX and the antisense sequences of miRNA-21.

■ ASSOCIATED CONTENT

Supporting Information

The Supporting Information is available free of charge on the ACS Publications website at DOI: 10.1021/jacs.5b10309.

Materials and detailed experimental procedures, supplementary figures (PDF)

3D nanopyramid reconstruction movie (MPG)

■ AUTHOR INFORMATION

Corresponding Author

*kuangh@jiangnan.edu.cn

Author Contributions

#These authors contributed equally.

Notes

The authors declare no competing financial interest.

■ ACKNOWLEDGMENTS

This work is financially supported by the National Natural Science Foundation of China (21471068, 31400848, 21371081, 21301073, 21471128).

■ REFERENCES

(1) Chen, Y.; Gao, D. Y.; Huang, L. *Adv. Drug Delivery Rev.* **2015**, *81*, 128.
(2) Devulapally, R.; Sekar, N. M.; Sekar, T. V.; Foygel, K.; Massoud, T. F.; Willmann, J. r. K.; Paulmurugan, R. *ACS Nano* **2015**, *9*, 2290.
(3) Pritchard, C. C.; Cheng, H. H.; Tewari, M. *Nat. Rev. Genet.* **2012**, *13*, 358.
(4) Bartel, D. P. *Cell* **2009**, *136*, 215.
(5) Liu, C.; Wen, J.; Meng, Y.; Zhang, K.; Zhu, J.; Ren, Y.; Qian, X.; Yuan, X.; Lu, Y.; Kang, C. *Adv. Mater.* **2015**, *27*, 292.
(6) Lu, J.; Getz, G.; Miska, E. A.; Alvarez-Saavedra, E.; Lamb, J.; Peck, D.; Sweet-Cordero, A.; Ebert, B. L.; Mak, R. H.; Ferrando, A. A.; Downing, J. R.; Jacks, T.; Horvitz, H. R.; Golub, T. R. *Nature* **2005**, *435*, 834.
(7) Lin, S.; Gregory, R. I. *Nat. Rev. Cancer* **2015**, *15*, 321.
(8) Git, A.; Dvinge, H.; Salmon-Divon, M.; Osborne, M.; Kutter, C.; Hadfield, J.; Bertone, P.; Caldas, C. *RNA* **2010**, *16*, 991.
(9) Degliangeli, F.; Kshirsagar, P.; Brunetti, V.; Pompa, P. P.; Fiammengo, R. *J. Am. Chem. Soc.* **2014**, *136*, 2264.
(10) Garcia-Schwarz, G.; Santiago, J. G. *Angew. Chem., Int. Ed.* **2013**, *52*, 11534.
(11) Jin, Z.; Geissler, D.; Qiu, X.; Wegner, K. D.; Hildebrandt, N. *Angew. Chem., Int. Ed.* **2015**, *54*, 10024.
(12) Causa, F.; Aliberti, A.; Cusano, A. M.; Battista, E.; Netti, P. A. *J. Am. Chem. Soc.* **2015**, *137*, 1758.
(13) Joshi, G. K.; Deitz-McElyea, S.; Johnson, M.; Mali, S.; Korc, M.; Sardar, R. *Nano Lett.* **2014**, *14*, 6955.
(14) Wu, Z.; Liu, G. Q.; Yang, X. L.; Jiang, J. H. *J. Am. Chem. Soc.* **2015**, *137*, 6829.
(15) Tay, C. Y.; Yuan, L.; Leong, D. T. *ACS Nano* **2015**, *9*, 5609.
(16) Yin, B. C.; Liu, Y. Q.; Ye, B. C. *J. Am. Chem. Soc.* **2012**, *134*, 5064.
(17) Yang, Y.; Huang, J.; Yang, X.; Quan, K.; Wang, H.; Ying, L.; Xie, N.; Ou, M.; Wang, K. *J. Am. Chem. Soc.* **2015**, *137*, 8340.
(18) Choi, C. K.; Li, J.; Wei, K.; Xu, Y. J.; Ho, L. W.; Zhu, M.; To, K. K.; Choi, C. H.; Bian, L. *J. Am. Chem. Soc.* **2015**, *137*, 7337.
(19) Asanuma, H.; Akahane, M.; Niwa, R.; Kashida, H.; Kamiya, Y. *Angew. Chem., Int. Ed.* **2015**, *54*, 4315.
(20) Halstead, J. M.; Lionnet, T.; Wilbertz, J. H.; Wippich, F.; Ephrussi, A.; Singer, R. H.; Chao, J. A. *Science* **2015**, *347*, 1367.
(21) Wu, C.; Cansiz, S.; Zhang, L.; Teng, I. T.; Qiu, L.; Li, J.; Liu, Y.; Zhou, C.; Hu, R.; Zhang, T.; Cui, C.; Cui, L.; Tan, W. *J. Am. Chem. Soc.* **2015**, *137*, 4900.
(22) Dong, H.; Lei, J.; Ju, H.; Zhi, F.; Wang, H.; Guo, W.; Zhu, Z.; Yan, F. *Angew. Chem., Int. Ed.* **2012**, *51*, 4607.
(23) Ryoo, S.-R.; Lee, J.; Yeo, J.; Na, H.-K.; Kim, Y.-K.; Jang, H.; Lee, J. H.; Han, S. W.; Lee, Y.; Kim, V. N. *ACS Nano* **2013**, *7*, 5882.
(24) Kim, P. Y.; Oh, J. W.; Nam, J. M. *J. Am. Chem. Soc.* **2015**, *137*, 8030.
(25) Xu, L.; Yan, W.; Ma, W.; Kuang, H.; Wu, X.; Liu, L.; Zhao, Y.; Wang, L.; Xu, C. *Adv. Mater.* **2015**, *27*, 1706.
(26) Giljohann, D. A.; Seferos, D. S.; Daniel, W. L.; Massich, M. D.; Patel, P. C.; Mirkin, C. A. *Angew. Chem., Int. Ed.* **2010**, *49*, 3280.
(27) Saha, K.; Agasti, S. S.; Kim, C.; Li, X.; Rotello, V. M. *Chem. Rev.* **2012**, *112*, 2739.
(28) Yang, X.; Yang, M.; Pang, B.; Vara, M.; Xia, Y. *Chem. Rev.* **2015**, *115*, 10410.
(29) Li, L. L.; Lu, Y. *J. Am. Chem. Soc.* **2015**, *137*, 5272.

DOI: 10.1021/jacs.5b10309
J. Am. Chem. Soc. 2016, 138, 306−312

(30) Chou, L. Y.; Zagorovsky, K.; Chan, W. C. *Nat. Nanotechnol.* **2014**, *9*, 148.
(31) Chinen, A. B.; Guan, C. M.; Ferrer, J. R.; Barnaby, S. N.; Merkel, T. J.; Mirkin, C. A. *Chem. Rev.* **2015**, *115*, 10530.
(32) Liang, L.; Li, J.; Li, Q.; Huang, Q.; Shi, J.; Yan, H.; Fan, C. *Angew. Chem., Int. Ed.* **2014**, *53*, 7745.
(33) Zhang, L.; Lei, J.; Liu, J.; Ma, F.; Ju, H. *Chem. Sci.* **2015**, *6*, 3365.
(34) Jung, S. H.; Jeon, J.; Kim, H.; Jaworski, J.; Jung, J. H. *J. Am. Chem. Soc.* **2014**, *136*, 6446.
(35) Lan, X.; Lu, X.; Shen, C.; Ke, Y.; Ni, W.; Wang, Q. *J. Am. Chem. Soc.* **2015**, *137*, 457.
(36) Li, Z.; Zhu, Z.; Liu, W.; Zhou, Y.; Han, B.; Gao, Y.; Tang, Z. *J. Am. Chem. Soc.* **2012**, *134*, 3322.
(37) Maoz, B. M.; van der Weegen, R.; Fan, Z.; Govorov, A. O.; Ellestad, G.; Berova, N.; Meijer, E. W.; Markovich, G. *J. Am. Chem. Soc.* **2012**, *134*, 17807.
(38) Shen, X.; Song, C.; Wang, J.; Shi, D.; Wang, Z.; Liu, N.; Ding, B. *J. Am. Chem. Soc.* **2012**, *134*, 146.
(39) Fan, Z.; Govorov, A. O. *Nano Lett.* **2012**, *12*, 3283.
(40) Kuzyk, A.; Schreiber, R.; Fan, Z.; Pardatscher, G.; Roller, E.-M.; Högele, A.; Simmel, F. C.; Govorov, A. O.; Liedl, T. *Nature* **2012**, *483*, 311.
(41) Querejeta-Fernandez, A.; Chauve, G.; Methot, M.; Bouchard, J.; Kumacheva, E. *J. Am. Chem. Soc.* **2014**, *136*, 4788.
(42) Wu, X.; Xu, L.; Liu, L.; Ma, W.; Yin, H.; Kuang, H.; Wang, L.; Xu, C.; Kotov, N. A. *J. Am. Chem. Soc.* **2013**, *135*, 18629.
(43) Yan, W.; Xu, L.; Xu, C.; Ma, W.; Kuang, H.; Wang, L.; Kotov, N. A. *J. Am. Chem. Soc.* **2012**, *134*, 15114.
(44) Ma, W.; Kuang, H.; Xu, L.; Ding, L.; Xu, C.; Wang, L.; Kotov, N. A. *Nat. Commun.* **2013**, *4*, 2689.
(45) Hou, Y.; Qiao, R.; Fang, F.; Wang, X.; Dong, C.; Liu, K.; Liu, C.; Liu, Z.; Lei, H.; Wang, F. *ACS Nano* **2012**, *7*, 330.
(46) Li, Z.; Lv, S.; Wang, Y.; Chen, S.; Liu, Z. *J. Am. Chem. Soc.* **2015**, *137*, 3421.
(47) Wang, L.; Dong, H.; Li, Y.; Xue, C.; Sun, L. D.; Yan, C. H.; Li, Q. *J. Am. Chem. Soc.* **2014**, *136*, 4480.
(48) Liu, J.; Liu, Y.; Bu, W.; Bu, J.; Sun, Y.; Du, J.; Shi, J. *J. Am. Chem. Soc.* **2014**, *136*, 9701.
(49) Wang, L.; Dong, H.; Li, Y.; Liu, R.; Wang, Y. F.; Bisoyi, H. K.; Sun, L. D.; Yan, C. H.; Li, Q. *Adv. Mater.* **2015**, *27*, 2065.
(50) Qiao, R.; Liu, C.; Liu, M.; Hu, H.; Liu, C.; Hou, Y.; Wu, K.; Lin, Y.; Liang, J.; Gao, M. *ACS Nano* **2015**, *9*, 2120.
(51) Cheng, L.; Yang, K.; Li, Y.; Chen, J.; Wang, C.; Shao, M.; Lee, S. T.; Liu, Z. *Angew. Chem., Int. Ed.* **2011**, *50*, 7385.
(52) Wu, S.; Butt, H. J. *Adv. Mater.* **2015**, DOI: 10.1002/adma.201502843.
(53) Haase, M.; Schafer, H. *Angew. Chem., Int. Ed.* **2011**, *50*, 5808.
(54) Liu, J.; Bu, J.; Bu, W.; Zhang, S.; Pan, L.; Fan, W.; Chen, F.; Zhou, L.; Peng, W.; Zhao, K.; Du, J.; Shi, J. *Angew. Chem., Int. Ed.* **2014**, *53*, 4551.
(55) Zhang, C.; Yang, L.; Zhao, J.; Liu, B.; Han, M. Y.; Zhang, Z. *Angew. Chem., Int. Ed.* **2015**, *54*, 11531.
(56) Liu, X.; Yan, C. H.; Capobianco, J. A. *Chem. Soc. Rev.* **2015**, *44*, 1299.
(57) Zhou, B.; Shi, B.; Jin, D.; Liu, X. *Nat. Nanotechnol.* **2015**, *10*, 924.
(58) Li, Z.; Lv, S.; Wang, Y.; Chen, S.; Liu, Z. *J. Am. Chem. Soc.* **2015**, *137*, 3421.
(59) Park, Y. I.; Lee, K. T.; Suh, Y. D.; Hyeon, T. *Chem. Soc. Rev.* **2015**, *44*, 1302.
(60) Cheglakov, Z.; Cronin, T. M.; He, C.; Weizmann, Y. *J. Am. Chem. Soc.* **2015**, *137*, 6116.
(61) Chan, H.-M.; Chan, L.-S.; Wong, R. N.-S.; Li, H.-W. *Anal. Chem.* **2010**, *82*, 6911.

DOI: 10.1021/jacs.5b10309
J. Am. Chem. Soc. 2016, 138, 306−312